ACTIVE INLET FLOW CONTROL TECHNOLOGY DEMONSTRATION

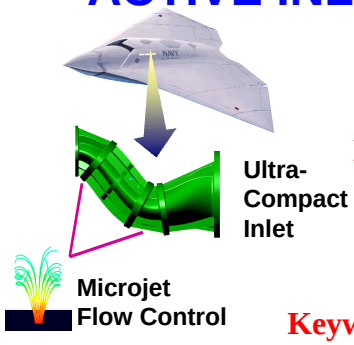

J.W. Hamstra, D.N. Miller, P.P. Truax
Lockheed Martin Aeronautics Company
E-mail: jeffrey.w.hamstra@lmco.com
B.A. Anderson, B.J. Wendt
NASA Glenn Research Center

Keywords: *Inlet, Flow Control, Microvane, Microjet*

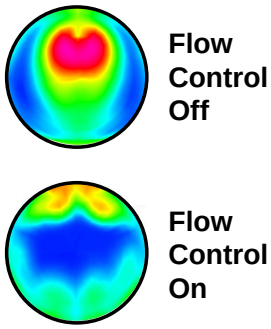

Abstract

This paper presents results from a joint Lockheed Martin/NASA Glenn effort to design and verify an ultra-compact, highly-survivable engine inlet subsonic duct based on the emerging technology of Active Inlet Flow Control (AIFC). In the AIFC concept, micro-scale actuation (~mm in size) is used in an approach denoted 'secondary flow control' to intelligently alter a serpentine duct's inherent secondary flow characteristics with the goal of simultaneously improving the critical system-level performance metrics of total pressure recovery, spatial distortion, and RMS turbulence. In this approach, separation control is a secondary benefit, not a design requirement. The baseline concept for this study was a 4:1 aspect ratio ultra-compact (L/D=2.5) serpentine duct that fully obscured line-of-sight view of the engine face. At relevant flow conditions, this type of duct exhibits excessive pressure loss and distortion because of extreme wall curvature. Two sets of flow control effectors were designed with the intent of establishing high performance levels to the baseline duct. The first set used two arrays of 36 co-rotating microvane vortex generators (VGs); the second set used two arrays of 36 micro air-jet (microjet) VGs, which were designed to produce the same 'vorticity signature' as the microvanes. Optimization of the microvane array was accomplished using a Design of Experiments (DOE) methodology to guide selection of parameters used in multiple Computational Fluid Dynamics (CFD) flow solutions. A verification test conducted in the NASA Glenn W1B test facility indicated low pressure recovery and high distortion for the baseline duct without flow control. With microvane flow control, at a throat Mach number of 0.60, pressure recovery was increased 5%, and both spatial distortion and turbulence were decreased approximately 50%. Microjet effectors also provided significantly improved performance over the baseline configuration.

Nomenclature

AIFC	Active Inlet Flow Control
AIP	Aerodynamic Interface Plane
c	Vane Chord Length
CCF	Central Composite Face
CFD	Computational Fluid Dynamics
D	Duct Diameter
DC(60)	Circumferential Distortion Parameter
DOE	Design of Experiments
ESP	Electronically Scanned Pressure
GRC	Glenn Research Center
h	Vane Height
L	Duct Length
LM	Lockheed Martin Aeronautics Company
MoD	Ministry of Defense
n	Number of Vanes Per Station
NASA	National Aeronautics and Space Administration
P	Pressure
Re	Reynolds Number
RMS	Root Mean Square
UAV	Unmanned Air Vehicle
VG	Vortex Generator
Xc	Lines Control Station Location
α	Vane Angle of Incidence
Subscripts:	
0	Freestream Conditions
2	Engine Face (AIP) Conditions
S	Surface
T	Total

1 Technical Need

Affordability, defined as the ratio of capability to cost, is becoming the dominant design requirement for future tactical aircraft. Affordability must be achieved, however, while simultaneously improving both survivability and aerodynamic performance. To meet vehicle affordability goals, future propulsion systems must be lighter, more compact, and must accommodate ever-increasing integration between the air vehicle, engine, and various subsystems (Figure 1). The engine inlet system shares these goals. However, inlet duct design parameters (offset, wall curvature rate, shaping,

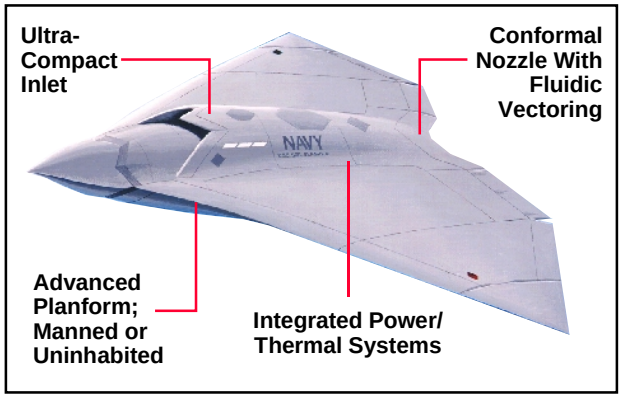

Figure 1: Future aircraft require advanced propulsion technologies to meet affordability goals

diffusion rate, etc.) are limited by considerations of pressure loss and flow non-uniformity (distortion). As future systems evolve toward more compact designs with exotic, survivability-driven shaping, these limitations will in turn limit the design space for the vehicle itself. A need thus exists for new technologies that can overcome these inlet design limitations.

AIFC technology offers one approach to satisfy this need. There are several essential elements comprising the authors' embodiment of AIFC, including: 1) the use of internally-generated co-rotating vortices to enact global control of secondary flow, rather than local control of separation (i.e. secondary flow control); 2) micro-scale control effectors; 3) optimizing to system-level flow metrics at the engine face, not local flow phenomena within the duct; 4) realistic flowpath lines and relevant Reynolds Number (Re) and Mach number conditions; 5) use of a coupled CFD/DOE development method; 6) the principle of 'vorticity signature' and use of a 'vorticity model' within the CFD code; and 7) the use of sensors and an adaptive, closed-loop control system. The current paper reports on efforts regarding the first six of these elements.

2 Previous & Ongoing Efforts

Historically, the most common method of flow control in inlet ducts has been the inclusion of vane or air-jet type VGs to 'locally' control the adverse effects of separation. Vorticity generation from the VGs is used to 'locally' mix low and high momentum regions in the flow, effectively spreading out the lower momentum fluid to suppress flow separation from the wall [1]. However, application of this flow control method to advanced serpentine inlet ducts does not necessarily achieve significant reduction of engine face distortion. Furthermore, the 'local' use of VGs only allows separation to be controlled at one flow condition (usually the cruise condition), with all other conditions rendered 'off-design.' More recent studies have similarly addressed control of separation in a 2-dimensional duct using pulsed or synthetic jets [2]. While reattachment of the separated flow is obtained, such studies are mainly of academic interest because they were conducted on simplistic flowpath geometry at very low Re conditions, demonstrating no direct benefit to inlet system-level metrics.

The use of VGs within the current study is viewed in a categorically different manner - the generators are used to 'globally' restructure the secondary flow for the purpose of increasing total pressure recovery and decreasing spatial distortion and RMS turbulence (Figure 2). More specifically, it is not the goal to prevent flow separation *per se*, unless such action produces an improvement in system-level metrics at the engine face. Anderson and Gibb [3] first proposed the concept of VGs as secondary flow control effectors. Initial elements of the AIFC concept were formally established by Anderson and Gibb [4], and verified by comparison with

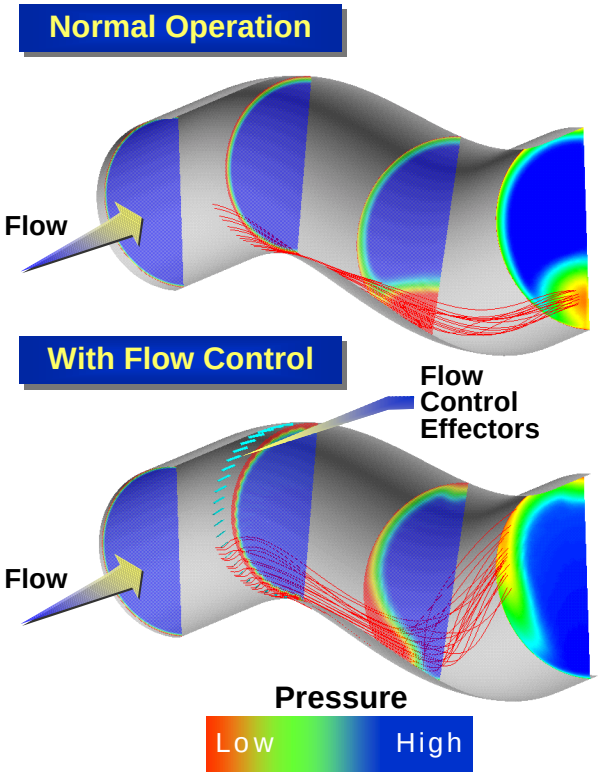

Figure 2: Secondary flow control can be used to tailor engine face distortion patterns

experimental data obtained in the DERA/Bedford 13x9 ft. wind tunnel. Gibb and Anderson [5] also demonstrated that, at moderate Reynolds numbers, the same performance gains could be achieved by replicating the vane-type effector array with air-jet VGs. Bray et al. [6] extended this verification to flight Reynolds numbers. This research, initiated under a NASA/Ministry of Defense (MoD) cooperative program, lead to the concept of a 'vorticity signature' equivalency principle. The principle states that the key element of secondary flow control is the overall vorticity strength, distribution, and secondary flow field interaction created by an effector array within the boundary layer. The actual source of vorticity, be it vane or air-jet VGs, is of much less importance. With this established, inlet flow control research has shifted from a concern for 'vane geometry' and 'preventing flow separation' to establishing the proper overall vorticity signature to optimize system-level metrics. Recognizing that inlet distortion is also a forcing function for vibration in the fan components, methods for reducing distortion-induced high cycle fatigue are also part of this research effort.

These concepts allow the formal application of an integrated CFD/DOE optimization procedure to design effector arrays while encompassing a wide variety of inlet operating conditions. The equivalency principle also simplifies modeling of effector arrays in full Navier-Stokes CFD analyses and provides a close agreement with experimental data even for a coarse grid calculation (Bender et al.[7]). CFD analysis was used by Anderson et al. [8] to successfully verify that micro-scale effector arrays can manage the entire inlet duct flow field by controlling the flow in a thin layer adjacent to the duct wall (about the thickness of the momentum layer). Within a research consortium composed of Lockheed Martin Aeronautics Company (LM), NASA Glenn Research Center (GRC), and the US Air Force Research Laboratories, current ongoing efforts on AIFC are focusing on micro-scale effectors in relevant, survivable, ultra-compact inlet configurations at realistic conditions.

3 Inlet Configuration Development

3.1 Baseline Flowpath Design

The baseline inlet flowpath for this study featured a high aspect ratio (4:1), biconvex-shaped entrance section with an ultra-compact (L/D = 2.5), dual-turn, serpentine duct that fully

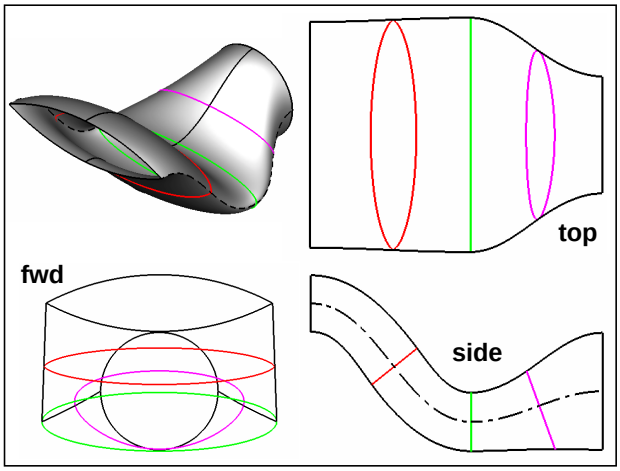

Figure 3: An advanced, serpentine, ultra-compact duct was chosen as the baseline concept

obscured view of the circular exit section (Figure 3). This type of duct is required for vehicles such as the all-wing, unmanned air vehicle (UAV) concept shown in Figure 1. For this design, planform length, and thus vehicle weight and cost, is directly proportional to duct length. Results of a scaling analysis on a similar vehicle showed a sensitivity of 15% empty weight for length reductions equivalent to one duct diameter. It is thus desirable to minimize duct length while retaining full-obscuration and high aerodynamic performance. Traditionally, this type of ultra-compact duct design would be excluded from consideration since it is characterized by severe wall curvature that induces strong secondary flows, resultant coalescence of the boundary layer on the inner wall, and subsequent vortex lift-off separation. Such phenomena produce unacceptable levels of pressure loss, flow distortion, and turbulence.

Design studies were first conducted using CFD to optimize the baseline duct's cross-sectional shape and flow area distribution before the flow control system was applied. A comparison of CFD-based wall pressure distribution is shown in Figure 4 for the baseline duct compared to an F-16 inlet. Even with optimization, the ultra-compact duct exhibits a much larger magnitude and rate of stream-wise wall pressure rise than that of the F-16 inlet, indicating the potential for massive flow separation and high losses.

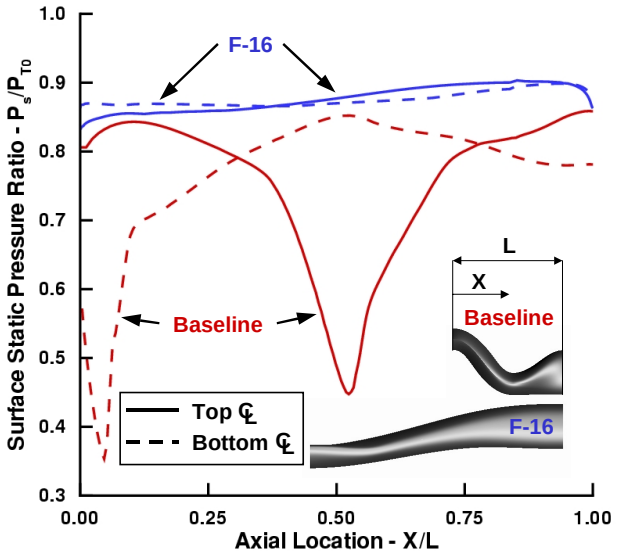

Figure 4: The baseline duct is characterized by severe internal pressure gradients

3.2 Microvane Effector Design Methodology

The flow control effector suites were conceptually developed with CFD methods using a DOE approach to investigate effects of both duct geometry and effector design variables on system-level performance metrics. This development process is outlined in Figure 5. DOE theory [9] provides a statistical design

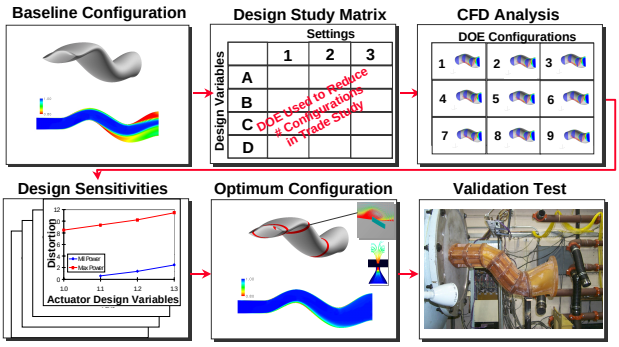

Figure 5: Control effector optimization was accomplished using a CFD/DOE process

technique that allows for the understanding of complex relationships between the design variables (or factors) and the decision metrics (or responses) set by project objectives. The DOE method is applied in the form of a predetermined design array that defines a series of experiments (combinations of design variables) that can evaluate the effects of each factor over its range of values. One array used in the research was the Central Composite Face (CCF) design. One such CCF array defines 45 'experiments' to evaluate the linear, quadratic, and interactive effects of six design factors at three settings each. A full permutation of such a system would require 3^6 or 729 experiments. CFD was used to predict the performance metrics for each of the 45 experiments.

The selected CFD solver was Falcon, a Reynolds-averaged Navier-Stokes code described by Miller et al. [10]. Falcon contains an advanced vorticity model [7] that allows numeric simulation of the microvane VGs without the need to physically embed the vane effectors in the CFD grid. The model allows

reductions in 3-dimensional grid size from ~4,000,000 points to ~500,000 points and computer run time by ~60%. During the study, several 'check cases' confirmed that CFD analysis results with the vorticity model and smaller grid matched results with the larger grid. Typical grid density for the larger grid solutions (with embedded microvanes) can be inferred from Figure 6.

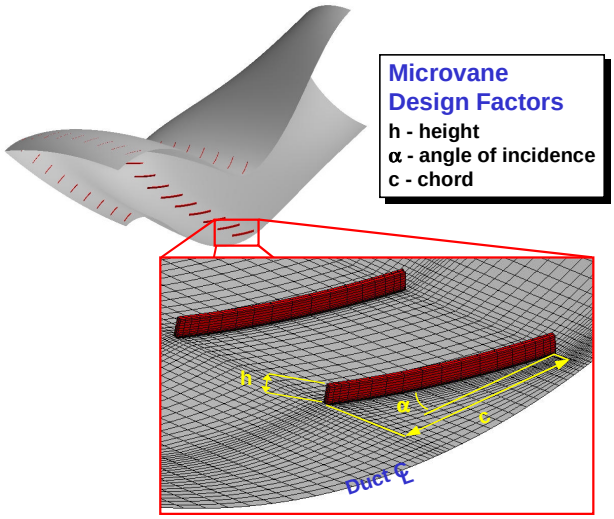

Figure 6: Microvane effector design factors

3.3 Flow Control Effector Suite Design

Two initial assumptions were made at the start of the microvane effector design process. The first assumption was that two arrays of effectors would be required: one array at the entrance to the first turn of the duct, and another array at the entrance of the second turn. The second assumption was that an interaction likely existed between the effector design and the basic duct geometry. DOE studies using CCF arrays were conducted to establish and optimize these relationships. Seven responses were measured for each study. The two responses with greatest weighting were duct total pressure recovery (P_{T2}/P_{T0}) and engine face distortion as indicated by DC(60), a common circumferential distortion descriptor [11]. The design factors for these DOE studies included vane height (h), chord to height ratio (c/h), vane angle-of-incidence (α), the number of vanes per station location (n), and the duct lines control station (Xc), which governed streamwise curvature of the duct. Several of these factors are illustrated in Figure 6. The effector variables were evaluated at stations corresponding to the first (forward) and second (rear) flowpath turns.

A strong interactive effect was encountered between Xc and the microvane effector parameters (Figure 7), suggesting that ultra-compact ducts of this type should be designed in conjunction with the effector array design. The results of these DOE studies substantiated the findings of Anderson, et al. [8] obtained for the M2129 inlet S-duct. Small (micro) vane heights controlled distortion level as well as conventional vanes (sized to the boundary layer thickness) but with more improvement to the total pressure recovery. Increasing vane angle-of-incidence and chord length had a strong beneficial effect on distortion and pressure recovery up to a critical level. Beyond this level, excessive vorticity was generated. The optimum design of the forward effector array was influenced by the design of the rear array.

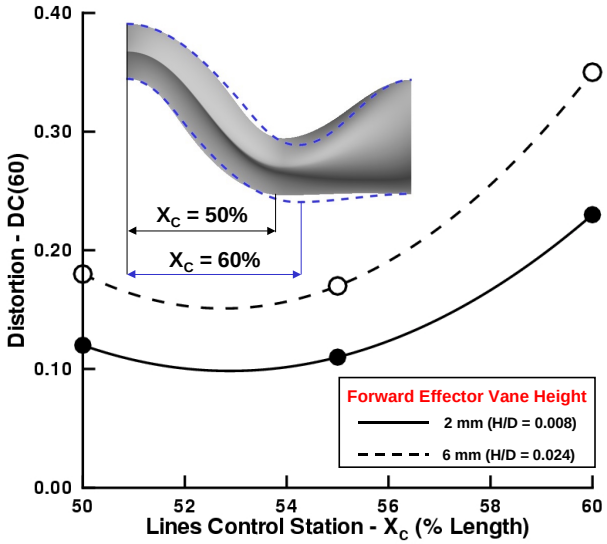

Figure 7: Example design factor sensitivities from the CFD/DOE process

The two arrays of microvane effectors were designed with the aforementioned methodology. Then, based on the equivalency principle, a set of microjet effectors were designed to produce the same vorticity signature.

4 Experimental Investigation

4.1 Model Design & Fabrication

A large-scale model of the AIFC duct geometry was designed and fabricated for test in the GRC W1B facility. The duct model was constructed entirely from resin using a laser stereo-lithography process. Although resin models can not achieve the same geometric fidelity and pressure and temperature ranges as metal models, they are much less costly. The test article was 63.5 cm long, and the aerodynamic interface plane (AIP) diameter was 25.4 cm, making the model approximately 40-50% scale for a UAV application. The model was designed in a modular fashion to accommodate both forward and aft effector arrays, or 'effector packs,' as shown in Figure 8. Effector pack modules for both microvanes (height ranging from 2-3 mm) and microjets (2 mm diameter) were fabricated. The test article was supplied air through a large area ratio, oval-to-biconvex bellmouth. A constant area section 25.4 cm in length was integrated between the bellmouth and the test article to develop a boundary layer thickness representative of that on an air vehicle forebody. Flanges with o-ring compression assemblies were designed into each module to avoid air leaks.

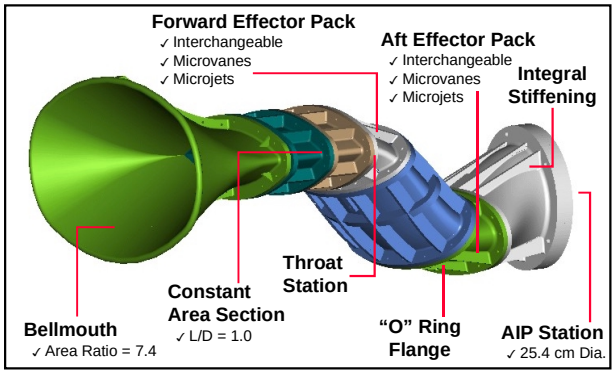

Figure 8: A modular test article was built from plastic resin using a laser stereo-lithography fabrication process

4.2 NASA GRC W1B Test Facility

The experimental verification test was conducted in the W1B Subsonic Diffuser Test Facility at NASA GRC in Cleveland, Ohio. The W1B facility and AIFC model installation are illustrated in Figure 9. Airflow at ambient atmospheric conditions entered the facility through a conical screen installed on the upstream end of a large plenum, which contained several internal screens and a honeycomb to condition the flow and reduce air turbulence. Flow exited the plenum through the model bellmouth. At the AIP, rake probes mounted in a cylindrical instrumentation duct were used to survey the flow field. Upon exiting the instrumentation duct, flow entered an altitude exhaust line and exited the facility. A plug valve located in this exhaust line regulated airflow through the test article. A downstream vacuum exhaust, continuously evacuated by remotely located compressors, drove the flow. The maximum mass flow through the test setup

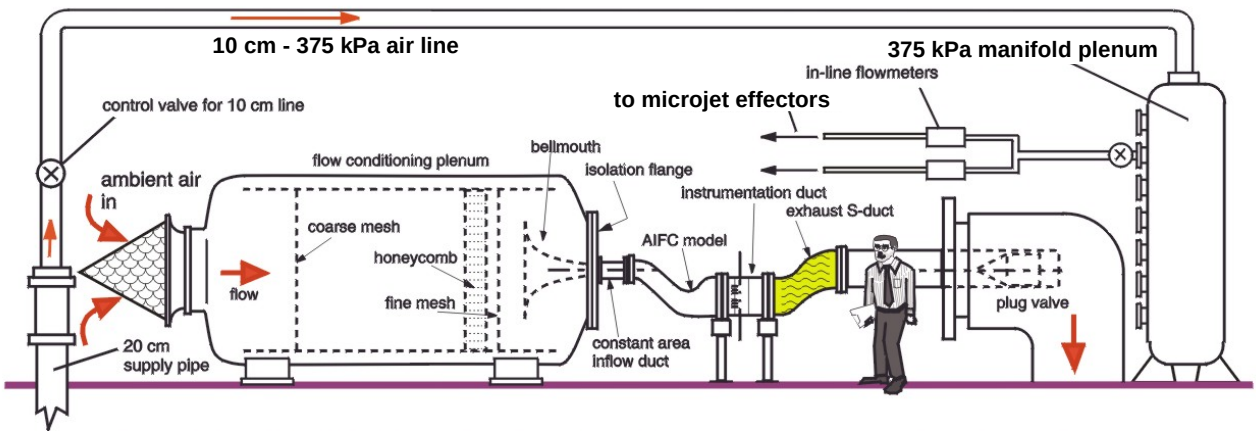

Figure 9: Schematic diagram of the NASA GRC W1B Subsonic Diffuser Test Facility in Cleveland, Ohio

was about 8 kg/s. Throat Mach number was the primary independent variable, and was varied from 0.43 to 0.68. Reynolds number, based on AIP diameter, was approximately $3x10^6$. Airflow through the microjet effectors was supplied by the high-pressure air system diagrammed in Figure 9. Shop air pressurized to about 2.5 atmospheres was routed to a large manifold plenum. A line leading from this plenum was split at a tee junction to supply both forward and aft microjet effector packs. A Flat-Trak Industrial In-Line Mass Flow Meter was installed on each branch to measure the mass flow through each effector pack. The overall flow rate through the system was controlled with a hydraulically actuated plug valve at the manifold plenum. Total microjet flow rates of up to 0.4 kg/s were possible.

4.3 Instrumentation & Data Acquisition

AIP instrumentation, wall static pressure taps, and boundary layer probes were included in the model. At the AIP, two radially translating 5-hole probe rakes acquired three components of the mean velocity, total pressure, and static pressure. Each rake consisted of three tips as diagrammed in Figure 10. Flow field measurements were acquired through translation of the 5-hole probe rakes and rotation of the AIP. The initial actuation was a radial traverse with step size of ~6.5 mm. The instrumentation

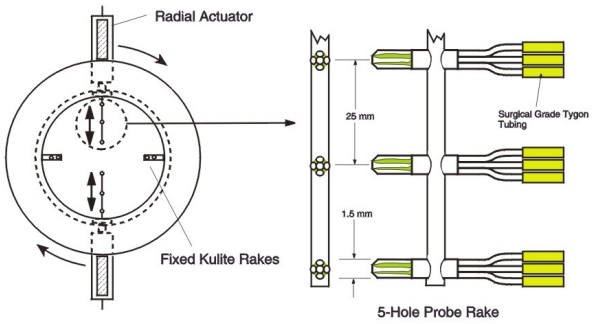

Figure 10: AIP instrumentation setup

ring was then manually rotated in 10° increments and the radial traverse repeated. This procedure provided a grid of 19 radial and 36 circumferential positions, or a total of 684 measurement points (Figure 11). Total pressure recovery and DC(60) distortion values were

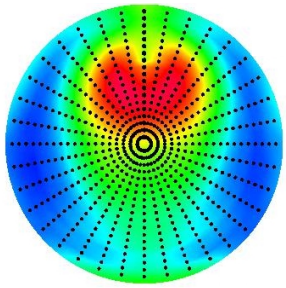

Figure 11: 684 AIP measurements were taken at 19 radial and 36 circumferential positions

calculated using the full set of AIP data. Two Kulite rakes were located at the AIP on a radial line 90° from the actuation axis of the 5-hole probe rakes. Each Kulite rake consisted of two radially fixed sensors calibrated to acquire the RMS turbulence of the flow field. The AIP actuation yielded a circular grid of 72 Kulite measurement points. Each measurement consisted of a time-average of 5 individual measurements acquired over approximately 20 seconds. Turbulence values were calculated as the simple average of the working transducers. Wendt and Reichert [12] included additional information on the construction, calibration, and use of this rake system. Boundary layer surveys were conducted near the throat of the model using a flattened Pitot probe. Normal actuation was conducted with a computer-driven Newport 5 centimeter-stroke actuator. Step sizes as small as 0.13 mm were employed. All pressures were sensed by an electronically-scanned pressure (ESP) transducer system.

4.4 Measurement Error Estimates

All pressures recorded with the ESP transducers are certain to within ± 15 Pa. Uncertainty in the pressure measurements recorded by the ESP transducers was used to derive total pressure uncertainty for the 5-hole probe rake system. The procedure accounts for the rake probe calibration and derived curve-fit routines [13]. The total pressures measured with the 5-hole probe rakes are certain to within ± 50 Pa over the full flow angle range of calibration (± 32 degrees in both pitch and yaw). The in-line flow meters used to measure mass flow rates to

the microjet effectors were factory calibrated. The uncertainty in mass flow rate measurement was about ±0.004 kg/s.

5 Experimental Test Results

Results from three test configurations are presented herein - the baseline duct without flow control (denoted as baseline), the baseline duct with microvane flow control (microvanes), and the baseline duct with micro air-jet flow control (microjets).

5.1 Baseline Configuration

A performance comparison of the baseline duct and a 'State-of-the-Art' advanced reference inlet is presented in Figure 12. Both pressure recovery and distortion characteristics for the baseline duct are significantly worse than those of the reference inlet. These differences are large enough that the baseline duct, without flow control, would not be considered for a realistic aircraft design.

An additional observation about the baseline duct is that the experimentally measured characteristics are significantly different than those predicted by CFD. This relationship can be seen in Figure 13 for both engine face patterns and longitudinal static pressure distributions. Comparison of the

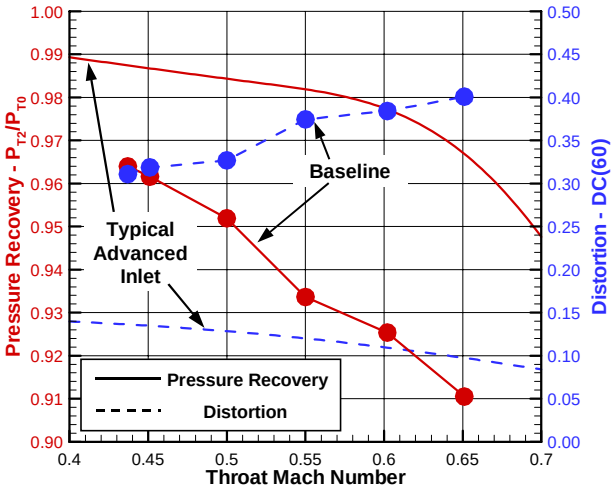

Figure 12: Baseline configuration performance (without flow control) compared to a 'typical advanced inlet'

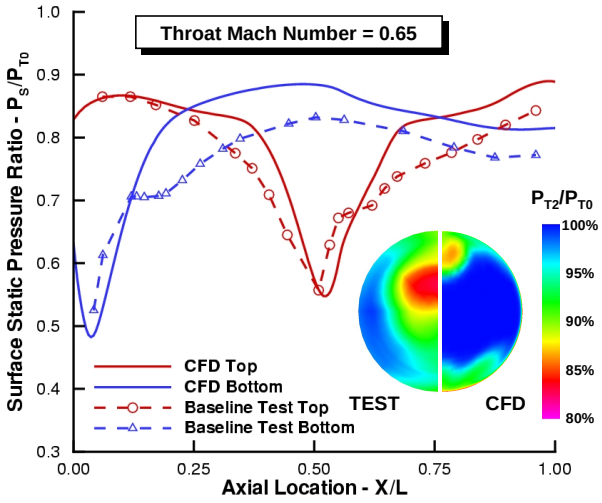

Figure 13: CFD analysis underpredicts pressure losses resulting from the highly-separated flow in the baseline configuration

engine face data shows that the classic vortex lift-off pattern is present in both cases; however, it is much stronger in the experimental case. The comparison of static pressure distribution again indicates an inability of the CFD code to predict the extreme degree of separation present in the duct. Previous studies of other inlet designs involving significant boundary layer separation have likewise noted this discrepancy. In all cases, the problem has been attributed to inadequacy in CFD solver turbulence models.

5.2 Microvane Devices

A comparison of pressure recovery, distortion, and RMS turbulence levels for the baseline, microvane, and microjet configurations is shown in Figure 14. The microvane configuration demonstrated dramatic improvement over the baseline configuration in both pressure recovery and turbulence over the entire tested range, and in distortion up to a throat Mach number of 0.60.

A comparison of CFD prediction and experimental data for the microvane configuration is show in Figure 15, with both engine face pattern and longitudinal static pressure distribution illustrated. In this case, the microvane effectors have controlled the flow separation, and the test data and CFD analysis

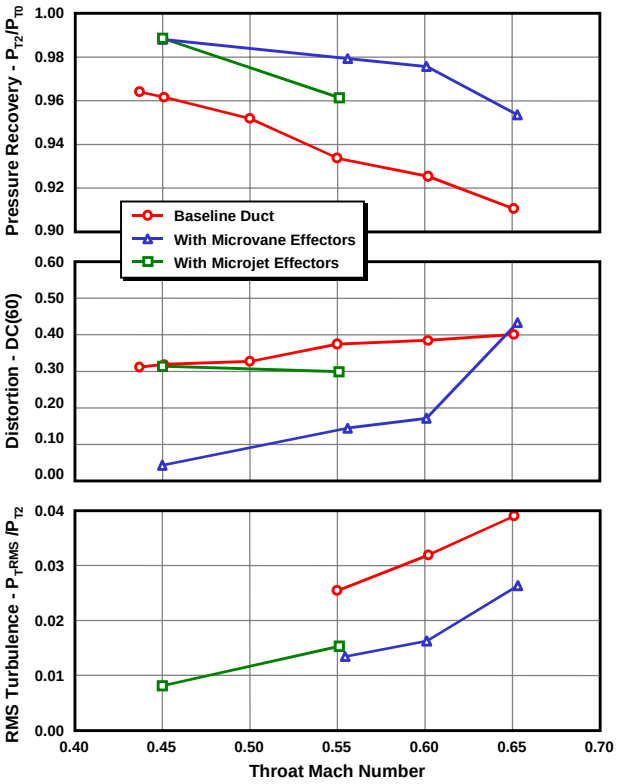

Figure 14: Performance metrics indicate significant improvement for both microvane and microjet effector configurations

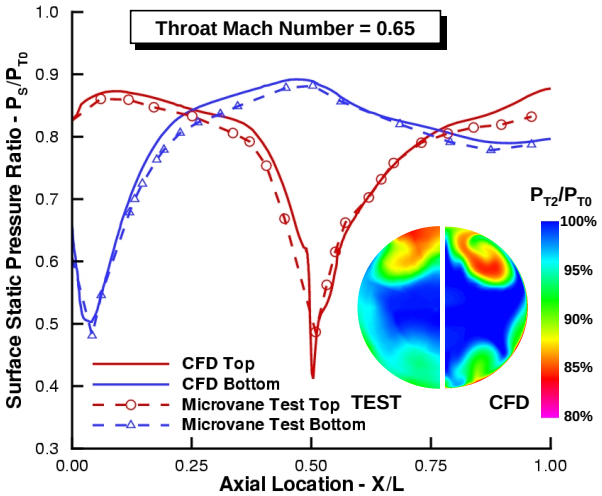

Figure 15: CFD analysis closely matches microvane configuration test data

compare very well. Taken together, the substantial performance improvement and favorable test-to-CFD comparison are interpreted as full verification of the microvane effector design methodology.

5.3 Microjet Devices

Results for the microjet configuration at a jet-to-primary flow ratio of 1% are also shown in Figure 14. The pressure recovery of the jet configuration is equal to the microvane configuration at a throat Mach number of 0.45. Above this throat Mach number the pressure recovery is between that of the microvane and baseline configuration, but in all cases, is a significant improvement over the baseline. Distortion improvement with the microjet effectors is not as good as the corresponding improvement shown for pressure recovery. There is some improvement (compared to the baseline) at throat Mach number of 0.55. The turbulence levels fall between those of the baseline and the microvanes. These trends are shown qualitatively in a comparison of engine face pressure patterns (Figure 16).

Although microjet performance was

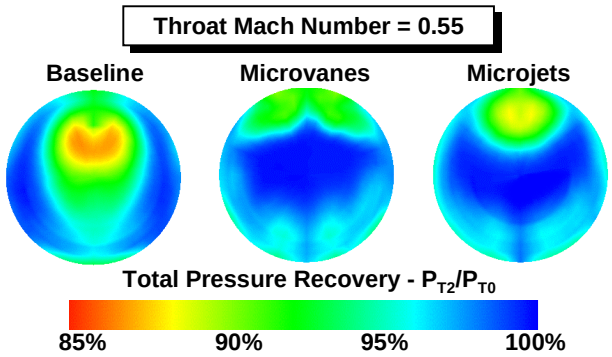

Figure 16: Microvane and microjet effectors produce similar distortion pattern improvement over the baseline

substantially better than baseline, it did not meet all expectations set by the vorticity signature design approach. The cause of this discrepancy is not yet well understood. However, it was noted that some re-work of the resin model parts was required during installation of the microjet effector packs. This re-work may have adversely impacted microjet effectiveness.

6 Summary & Conclusions

- Future tactical aircraft will likely require ultra-compact inlet subsonic duct systems with exotic, survivability-driven shaping.

These inlet systems cannot be achieved with current design technology. Active Inlet Flow Control (AIFC) offers a high-potential method for addressing this need.

- A CFD/DOE-based control effector design methodology was presented. This methodology allowed flow control effector optimization with only a fraction of the design effort required by traditional techniques.
- A large-scale experimental verification of AIFC was conducted on a realistic flowpath configuration at relevant Re and throat Mach number conditions
- Substantial improvement in all inlet system-level metrics was shown for the microvane effectors across the tested range In particular, total pressure recovery was increased by as much as 5%, and DC(60) distortion and RMS turbulence were decreased by as much as 50%.
- Viable flow control at relevant conditions can be achieved with micro-scale effectors – mm-sized devices with a characteristic dimension similar to the momentum layer thickness
- Experimental results compared well with CFD in cases with flow control. Without flow control, CFD under predicted separation, pressure loss, and distortion.
- Microjet effectors did not perform as well as microvane effectors. Additional investigation is required to determine if this was due to a model fabrication anomaly or to a need to redesign the microjets to better generate the scale of vorticity of the microvanes.

Acknowledgments

The authors acknowledge contributions of the following: Thomas Biesiadny of NASA GRC for support of this joint project; Skip Gridley of the Air Force Research Laboratory for guidance and support; Patrick Yagle and Erich Bender of LM for outstanding CFD analysis; Ray Arnold of LM for leading the AIFC model design; and David Hassinger and Brian Lundy of LM for assistance with data reduction and preparation of this manuscript.

References

[1] Tindell R H. Highly compact inlet diffuser technology. *AIAA Paper No. 87-1747*.

[2] Amitay M, Pitt D, Kibens V, Parekh D and Glezer A. Control of internal flow separation using synthetic jet actuators. *AIAA Paper No. 2000-0903*.

[3] Anderson B H and Gibb J. Study on vortex generator flow control for the management of inlet distortion. *Journal of Propulsion and Power*, Vol. 9, No. 3, pp 420-430, 1993.

[4] Anderson B H and Gibb J. Vortex generator installation studies on steady state and dynamic distortion. *Journal of Aircraft*, Vol. 35, No. 4, pp 513-552, 1998.

[5] Gibb J and Anderson B H. Vortex flow control applied to aircraft intake ducts. *Proceedings of the Royal Aero. Society*, Conf. Paper No. 14, 1995.

[6] Bray T P, Wier B and Gibb J. Experimental evaluation of inlet distortion management at flight Reynolds Number. *DERA/MSS/MSFC2/CR990134*, 1999.

[7] Bender E E, Anderson B H and Yagle P J. Vortex generator modeling for Navier-Stokes codes. *ASME Paper No. FEDSM99-69219*.

[8] Anderson B H, Miller D N, Yagle P J and Truax P P. A study on MEMS flow control for the management of engine face distortion in compact inlet systems. *ASME Paper No. FEDSM99-6920*.

[9] Box E P, Hunter W G and Hunter J S. *Statistics for experimenters*. John Wiley & Sons, 1978.

[10] Miller D N, Yagle P J and Hamstra J W. Fluidic throat skewing for thrust vectoring in fixed-geometry nozzles. *AIAA Paper No. 99-0365*.

[11] Hercock, R G and Williams D D. Aerodynamic response. *AGARD-LS-72*, Paper 3, 1974.

[12] Wendt B J and Reichert B A. An inexpensive and effective five-hole probe rake. *Experiments in fluids*, Vol. 19, pp. 295-296, 1995.

[13] Reichert B A and Wendt B J. Uncertainty of five-hole probe measurements. *Fluid Measurement and Instrumentation*, Vol. 183, pp 39-44, 1994.